Surface structure evolution and Raman response for multipulse, few-cycle, laser damaged ZnSe

YINGJIE CHAI,[1] [ORCID] XIAOMING YU,[1] HE CHENG,[1] ZENGHU CHANG,[1,2,3] LAURENE TETARD,[4,5] MICHAEL BASS,[1,2] AND M. J. SOILEAU[1,2,3,6,*]

[1] *CREOL, The College of Optics & Photonics, University of Central Florida, 4304 Scorpius Street., Orlando, FL 32816, USA*
[2] *Department of Physics, University of Central Florida, 4111 Libra Drive, Orlando, FL 32816, USA*
[3] *Institute for the Frontier of Attosecond Science and Technology, University of Central Florida, 4000 Central Florida Blvd, Orlando, FL 32826, USA*
[4] *Nanoscience Technology Center, University of Central Florida, 12424 Research Parkway, Orlando, FL 32826, USA*
[5] *Department of Materials Science and Engineering, University of Central Florida, 12760 Pegasus Drive, Orlando, FL 32816, USA*
[6] *Department of Electric and Engineer and Computer Science, University of Central Florida, 4328 Scorpius Street, Orlando, FL 32816, USA*
*mj@ucf.edu

Abstract: Multiple 11-fs infrared, few-cycle laser pulses were applied to a polycrystal ZnSe surface to study the evolution of surface damage morphologies. The polycrystalline grain boundaries seem to be the initiation site of surface damage and formation of ripples, which evolve as the result of many laser pulses at the same site. Scanning electron microscopy and atomic force microscopy (AFM) were applied to characterize the surface. The crystalline change and material phase transition were examined by confocal Raman spectroscopy. The thermal expansion coefficient increased slightly in the ablated zone compared to the non-ablated zone according to an AFM thermal tip test. The results show the growth and organization of surface ripples and the change of thermal properties as the number of irradiations at each site increases.

1. Introduction

Few-cycle laser interaction with optic components provides a way to study various phenomena including laser-induced carrier dynamics [1,2], laser-damage resistance [3–5], and high-harmonic generation [6–8]. They may have potential applications in high-density memory recording by taking advantage of the amorphous/crystalline phases. These phenomena have been explored using many-cycle infrared laser pulses (such as ~170 fs at 1030 nm), for a wide set of semiconductors, such as Si [9], Ge [10–14], and binary compound semiconductors, such as GeSb, GaAs, InSb, and InP [15]. The word of J. Bonse presented a comprehensive review of laser-induced ripples and various models proposed to explain such structures [12]. Few-cycle laser-induced material phase transition was not investigated in ZnSe, a very important material in the 0.4-15 micron region. Our previous work dealt with the interaction of a single 11 fs, 1.7 μm centered, few-cycle pulse with a ZnSe surface [16]. ZnSe material based gain media is usually exposed to multi-pulse in the laser systems [17,18]. Multiple pulse-induced laser damage behaviors must be investigated to check the accumulation effects and their sub-threshold effects on ZnSe material properties, such as crystalline state and stress properties. In this work, changes in the surface morphologies and crystalline structure were investigated for polycrystalline ZnSe, employing scanning electron microscopy, atomic force/thermal microscopy, and confocal Raman spectroscopy. The objectives

of this study were: first, to identify the surface structural alterations formed when pulse number increases and second, to evaluate changes to the material within the subsurface of the region exposed to many laser pulses. The laser-induced surface structure on a solid was widely accepted as resulting from the interaction between the incident light and induced surface waves as detailed in the extensive review in Ref. [12]. Owing to the recent development of ultrashort lasers, few-cycle laser sources have opened a new opportunity to observe laser-induced highly excited surface damage, occurring within the few femtosecond pulses. Experimental studies were designed to investigate the influence of multi-shot few-cycle laser pulses on the damage behavior of a ZnSe surface.

2. Experiments

2.1. Few-cycle laser-induced damage

11-fs, wide spectrum (central wavelength 1.7μm, the wavelength range of 1.2-2.2 μm) [18], infrared few-cycle laser pulses were applied in our experiment, as described in Fig. 1(A). N-on-1 laser-induced damage threshold (LIDT) measurements were implemented following ISO 21254, by increasing the shot number N. Focusing was achieved using an off-axis parabola. The focal spot had a $1/e^2$ diameter of 932.0 μm, forming an almost circular spot on the ZnSe surface. A real-time inspection of the irradiated area was done using an optical microscope. Table 1 shows that, as can be expected, the N-on-1 laser-resistance decreases rapidly as the number of pulse N increases, which demonstrates the existence of a damage accumulation effect. Figures 1(B)-(E) shows images of four representative craters ablated at the same fluence but using different numbers of pulses. A ring of the re-solidified material near the edge of the crater (called the "rim") is formed when a fluence is used that is higher than the LIDT given in Table 1.
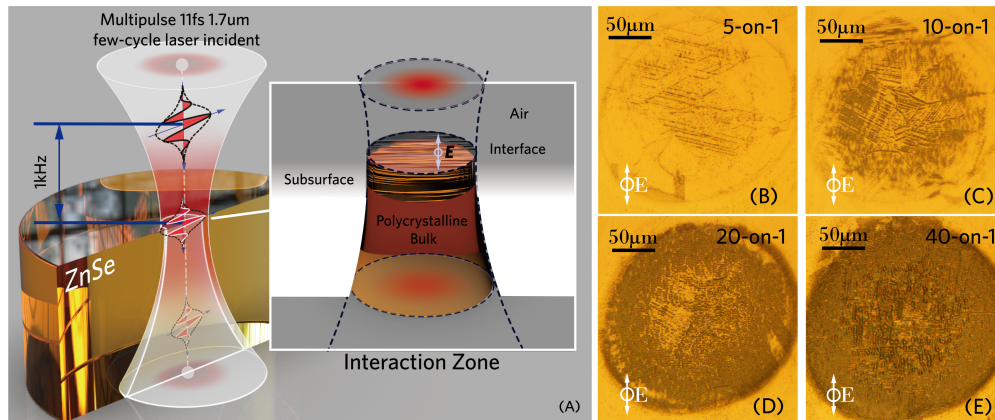

Fig. 1. (A) Schematic demonstration of few-cycle laser interaction with the ZnSe surface. The polycrystalline nature makes the surface easily modified by high E-field. 42 mJ/cm^2 11 fs few-cycle laser damage morphologies with shot number of (B) 5-on-1; (C) 10-on-1; (D) 20-on-1; (E) 40-on-1. The white E arrows denote the E-field polarization direction.

Table 1. Laser-induced damage (mJ/cm^2, 11fs, 0°)

Shot number	1	5	10	20	40
LIDT	89 ± 9	41 ± 4	28 ± 3	13 ± 1	10 ± 1

With 5 pulses, randomly oriented surface grooves were observed in the ablation area, which resulted from the polycrystalline nature of the materials [17]. By comparison of the scanning

electron microscope (SEM) images of Fig. 2 surface structure develops from randomly distributed grooves into well-oriented ripples when pulse number increases. A more detailed characterization of topographical changes in the laser-ablated area was performed utilizing an atomic force microscope (AFM) in tapping mode, as showed in Fig. 3. The sample surface was covered with a high density of redeposited material (debris) from the ablation process. The morphologies evolved from different orientations of the polycrystalline grains, into well-oriented ripples that are normal to the laser E-field. These ripples have a wavelength of ∼1.5 µm, as seen in Fig. 2(C). With low pulse number or weak irradiation intensity, the initial laser-induced structures were surface cracks with random orientations and crack distances, as shown in Fig. 2(A). Figure 2(B) showed that the ripple structures start as the crystalline boundaries with the polarization field induced by the component of the incident field normal to those structures. A well-oriented ripple pattern was observed when larger pulses number or stronger irradiation was employed: as extracted in Fig. 4, a well-oriented ripple with a period of ∼1.5 µm was gradually identified and the orientation of ripples became orthogonal to the incident E-field. We observed the ripple structure evolution by increasing the shot number in Fig. 2 (from left to right). The largest surface polarization component and thus the most efficient ripple generation is obtained for structures arrayed normal to the impressed E-field [10–12].
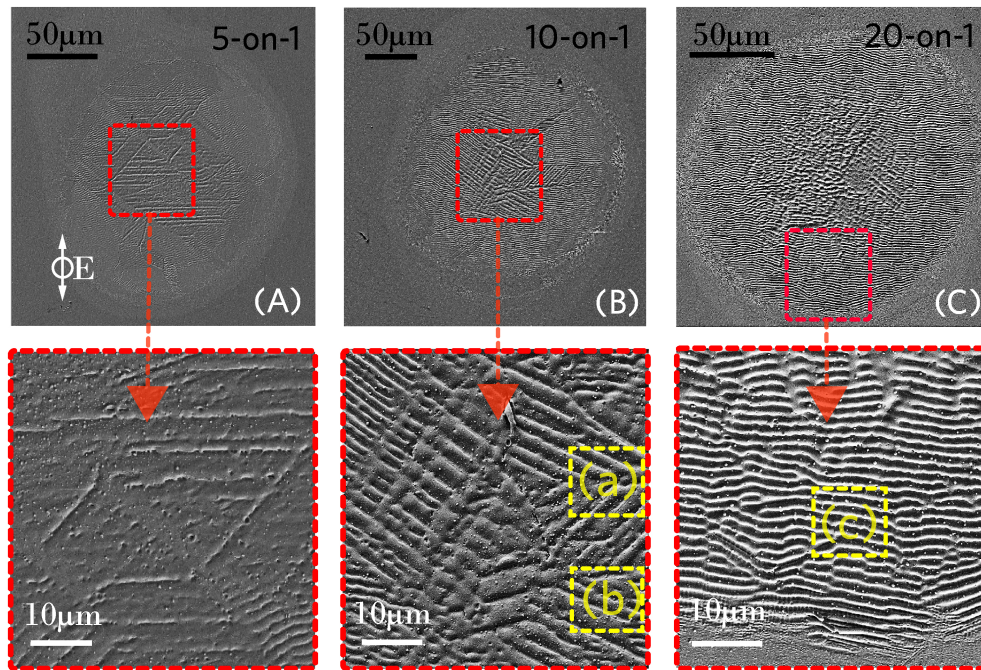

Fig. 2. SEM image comparison of 42 mJ/cm^2 11 fs few-cycle laser damage morphologies with shot number of (A) 5-on-1; (B) 10-on-1; and (C) 20-on-1. Red dot square denotes the enlarged view of the damaged area. The yellow dot square denotes the chosen AFM characterized position in the following figures.

The entire laser-induced damage process can be described as: first few pulses exposed the structure of the ZnSe subsurface grain boundaries. The structures were similar to that found when comparing the initially exposed damage cracks with the chemically etched ZnSe surface [19–22]. Exposed grain boundaries are seen as an e-field disturbance source to generate surface waves [11,12,23,24]. The enhanced surface E-field was produced by the polarization charge
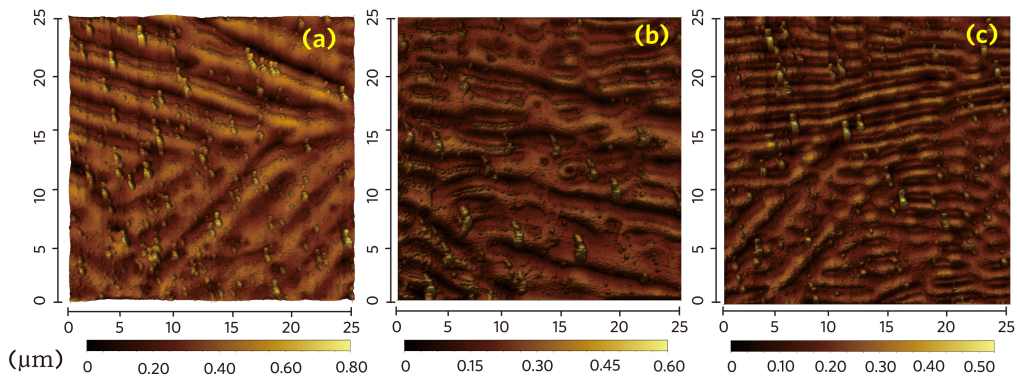
Fig. 3. AFM profiles of the marked zone in Fig. 2. (a) and (b) show the intermediate morphologies with a mixture of ZnSe crystalline grains and laser-induced ripples. (c) show the well-oriented laser-induced ripples after multiple pulse laser irradiation.
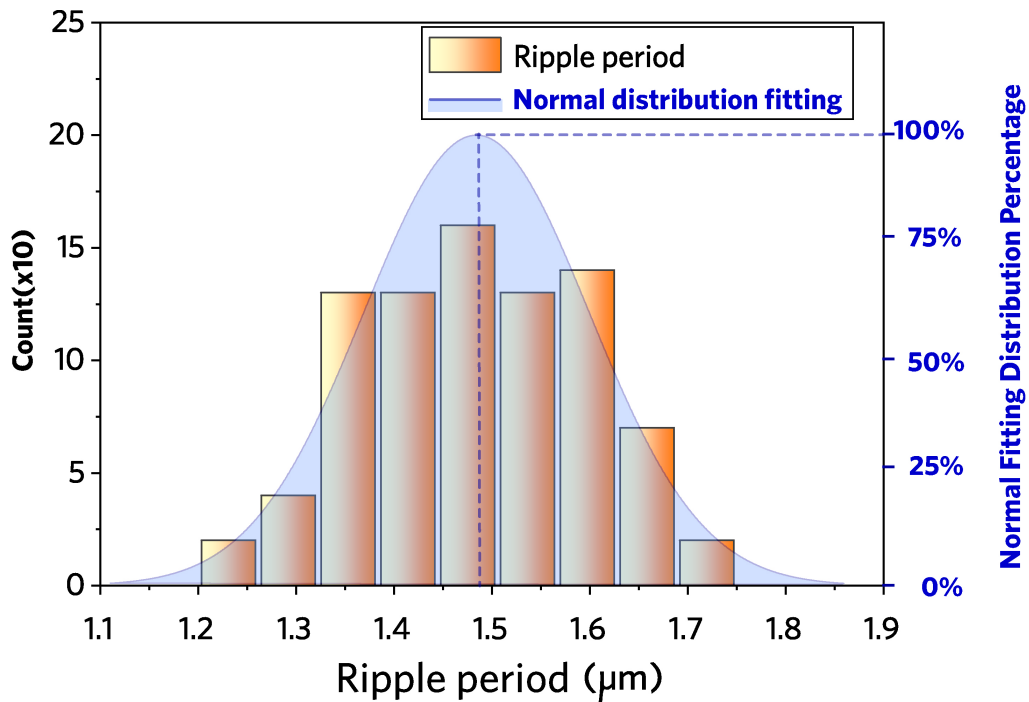

Fig. 4. Laser-induced ripple period distribution in the ablated zone, extracted from AFM test results. Normal distribution was fitted for an average period located at ~1.5μm.

introduced by surface discontinuities [24]. On the other hand, grain boundaries have a lower bandgap than the single crystal bulk [20,21]. The crystal near grain boundaries is more easily damaged by ionization breakdown than it would have if no grain boundary were present [25,26]. The polycrystalline nature turns the grain boundary into the most vulnerable part when laser irradiated.

2.2. Confocal Raman spectroscopy on an ablated area

Raman spectroscopic measurements were performed to investigate the crystal properties of the different observed zones, Confocal Raman spectral analysis was performed in the position of the non-ablated surface, ablated surface, and rippled surface. Figure 5(B) shows the spectra between 100 and 400 cm^{-1}, obtained at the location identified in Fig. 5(A). The phonon at the Brillouin zone center in the zinc blende structure ZnSe is split into a doubly degenerate transverse optical (TO) and longitudinal optical (LO) mode. The Raman spectrum of the original ZnSe surface and damaged ZnSe surface is presented in Fig. 5(B). A significantly altered Raman spectrum was obtained from locations within the outer zone inside the gaussian spot size (position A), as well as the rippled central area (position B). We found sharp peaks at 255 cm^{-1} and 205 cm^{-1}, corresponding to LO modes and TO modes of the ZnSe crystal, respectively. The presence of the LO- and TO-phonon modes indicates the crystalline structure of the material near the surface is in good agreement with the data found in the literature [26]. Figure 5(B) shows no wavenumber shifting in the first-order optical phonons (TO or/and LO) within the experimental error of this configuration. No wavenumber shift indicates no localized residual stress change after laser irradiations. The LO/TO intensity variation was related to the localized crystallographic orientation [27]. From the Raman selection rules, one can conclude that the N-on-1 laser pulses initially melt the ZnSe which then re-solidifies in a polycrystalline state with statistically distributed crystallite orientations. The disorder of the polycrystalline sample is evident by the full-width-at-half-maximum (FWHM) of the peak, as found by Yu et. al [28]. FWHM of TO/LO showed no broadening before and after laser irradiation indicating no crystalline size change. This result confirms that the surface does not transform into an amorphous state. The intensity of the Raman scattered IR depends on the Raman tensor, which is related to crystal symmetry as:

$$I_R = |\vec{e}_i R(\gamma_{ij})\vec{e}_s|$$

Here $\vec{e}_i$ and $\vec{e}_s$ are the polarization of incident E-field and that of the scattered light. In our test, an incident $\vec{e}_i$ can be considered as a constant during the test. Concerning the Raman selection rules, the LO mode is allowed from the (100) plane in the x(-)x configuration, while the TO mode is not allowed in this configuration. The Raman bands from the non-ablated ZnSe surface show that the LO mode is active (represents an intense peak) while TO intensity is weak. The selection rule indicates that the majority of the crystallites have a [111] orientation. In the Raman scattering configuration, the high-intensity LO mode scattering indicates that the wave vectors $\vec{k}_i$ and $\vec{k}_s$ are mostly parallel to the [111] axis. To comply with the photon-phonon wave-vector conservation rule, the wave vector of the phonon excited in the Raman process must also be parallel to the X-axis. Thus, the displacement of the LO phonons was along the [111] axis and the displacement of the TO phonons was perpendicular to the [111] axis. The Raman spectrum of the few-cycle laser damaged zone showed the changes in the intensity of the LO and TO peaks when multi-pulses laser irradiation.

   In this case, the TO phonon mode is gradually allowed in the Raman scattering from the original orientation, which confirms that the few-cycle laser ablation exposed a new polycrystalline structure with new crystalline orientations (other than the [111] orientation) which has no dependence on incident laser polarization. It has been attributed to lattice disordering effects induced by purely electronic excitation at extremely large carrier generation rates. Such excitation can be induced by ultrashort laser pulses with a duration smaller than the electron-phonon
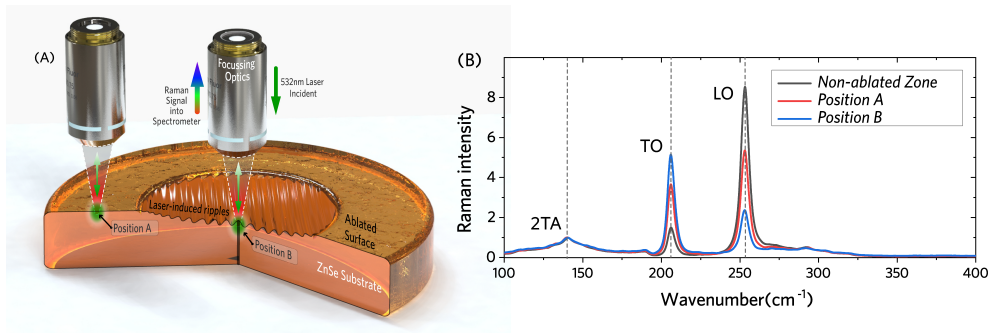
Fig. 5. On 10-on-1 damage site with 42 mJ/cm^2 irradiation: (A) Schematic of confocal Raman test position. (B) Confocal Raman spectroscopy results on ZnSe bulk (Non-ablated zone) and N-on-1 damage site. Shown are the TO 205 cm^{-1} and LO 251 cm^{-1} Raman spectra. The weaker peak (~139cm^{-1}) is attributed to the 2TA mode.

interaction time. However, according to the Raman spectroscopy, ultrafast phase transition ("non-thermal melting from polycrystalline into amorphous") has not been observed in the Raman spectroscopy test. The few-cycle irradiated area remains polycrystalline.

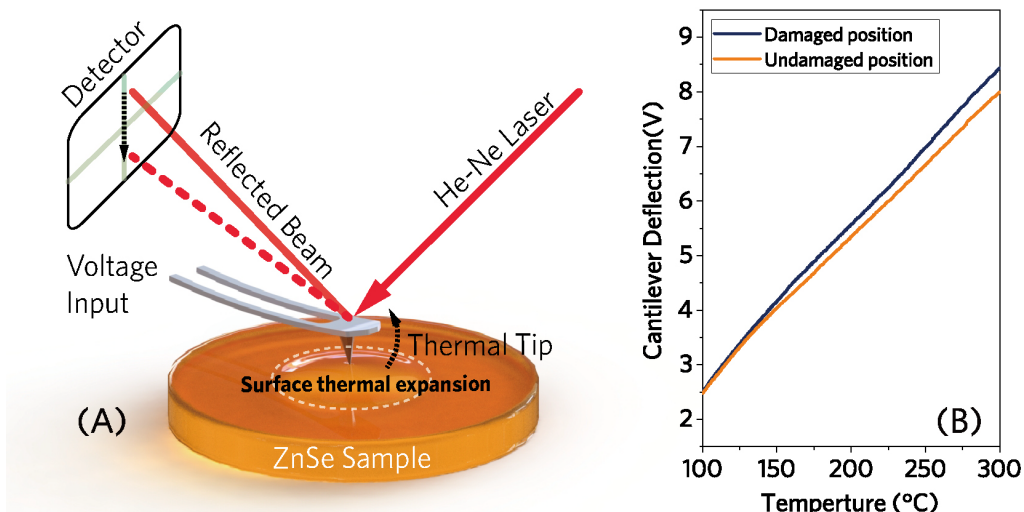### 2.3. Localized thermal response on an ablated area

Fig. 6. (A) Schematic of localized thermal response test by cantilever deflection variation induced by surface thermal expansion difference. A He-Ne Laser source was employed (same as AFM) and the tip temperature change was induced by an electric current. (B) Localized thermal response difference on the ZnSe surface with/without laser irradiation.

Crystal orientation variation can induce a change of localized physical property [29]. An AFM contact mode image was acquired, and the local thermal properties of the material were probed, using Nanoscale Thermal Analysis (nanoTA) [30]. The thermal probe was a ThermaLever Probes AN2-200, with a maximum controllable temperature limit of 350°C). The thermal probe was positioned on the target position to start the thermal response measurement, as sketched in Fig. 6(A). As the temperature of the probe is increased by applying a bias to the probe, the

deflection of the AFM cantilever is monitored to assess the thermal expansion of ZnSe. The thermal expansion coefficient of ZnSe with/without damage was different as shown in Fig. 6, especially above 150 °C. The figure indicates the damaged position showed a little higher thermal expansion coefficient than the undamaged position. The laser ablation created a structure with a different localized thermal response. We speculate reasonably that the re-solidification induced a small increase of the localized thermal expansion coefficient.

3. Conclusion

In this paper, we examined the material surface damage morphology and Raman spectroscopy response on the multi-pulse, 11 fs, few-cycle, laser-irradiated ZnSe surface. N-on-1 laser damage resistance decreased as the pulse number N increased, and cumulative damage was observed. We described the damage process phenomenologically: with the accumulation of short pulses' interactions, laser-induced structures gradually evolved to become orthogonal to the incident laser E-field polarization, as the most favorable condition for surface polarization-wave generation (as predicted in the model by Temple and Soileau (Ref. [23]) and other models reviewed in Ref. [12]). Confocal Raman spectroscopy showed that no ultrafast phase transition (from polycrystalline into amorphous) was induced by 11 fs ultrashort laser pulses used in the experiment. The thermal expansion coefficient slightly increased in the ripple zone over that in the non-ablated zone according to the AFM thermal tip test. Our work provides potential evidence for surface waves research and laser-induced crystalline phase changes. Future studies will be extended to single-crystalline ZnSe and other infrared materials to increase our understanding of few-cycle laser pulse's interactions.

References

1. Y. Chai and M. Soileau, Electron dynamic analysis of few-cycle laser-induced damage (Conference Presentation), in: *Laser-induced Damage in Optical Materials 2019, International Society for Optics and Photonics*, 2019, pp. 111730C.
2. P. Zhokhov and A. Zheltikov, "Optical breakdown of solids by few-cycle laser pulses," Sci. Rep. **8**(1), 1824 (2018).
3. V. Gruzdev and O. Sergaeva, "Ultrafast modification of band structure of wide-band-gap solids by ultrashort pulses of laser-driven electron oscillations," Phys. Rev. B **98**(11), 115202 (2018).
4. N. Sanner, O. Utéza, B. Chimier, M. Sentis, P. Lassonde, F. Légaré, and J. Kieffer, "Toward determinism in surface damaging of dielectrics using few-cycle laser pulses," Appl. Phys. Lett. **96**(7), 071111 (2010).
5. K. R. Kafka, N. Talisa, G. Tempea, D. R. Austin, C. Neacsu, and E. A. Chowdhury, "Few-cycle pulse laser induced damage threshold determination of ultra-broadband optics," Opt. Express **24**(25), 28858–28868 (2016).
6. T. Brabec and F. Krausz, "Intense few-cycle laser fields: Frontiers of nonlinear optics," Rev. Mod. Phys. **72**(2), 545–591 (2000).
7. P. Zhokhov and A. Zheltikov, "Field-cycle-resolved photoionization in solids," Phys. Rev. Lett. **113**(13), 133903 (2014).
8. E. Smetanina, P. G. de Alaiza Martínez, I. Thiele, B. Chimier, A. Bourgeade, and G. Duchateau, "Optical Bloch modeling of femtosecond-laser-induced electron dynamics in dielectrics," Phys. Rev. E **101**(6), 063206 (2020).
9. K. Werner, V. Gruzdev, N. Talisa, K. Kafka, D. Austin, C. M. Liebig, and E. Chowdhury, "Single-Shot Multi-Stage Damage and Ablation of Silicon by Femtosecond Mid-infrared Laser Pulses," Sci. Rep. **9** 19993 (2019).
10. J. F. Young, J. Preston, H. Van Driel, and J. Sipe, "Laser-induced periodic surface structure. II. Experiments on Ge, Si, Al, and brass," Phys. Rev. B **27**(2), 1155–1172 (1983).
11. J. F. Young, J. Sipe, and H. Van Driel, "Laser-induced periodic surface structure. III. Fluence regimes, the role of feedback, and details of the induced topography in germanium," Phys. Rev. B **30**(4), 2001–2015 (1984).

12. J. Bonse, S. Höhm, S. V. Kirner, A. Rosenfeld, and J. Krüger, "Laser-induced periodic surface structures—A scientific evergreen," IEEE J. Sel. Top. Quantum Electron. **23**, STh1Q.3 (2016).

13. M. Huang, F. Zhao, Y. Cheng, N. Xu, and Z. Xu, "The morphological and optical characteristics of femtosecond laser-induced large-area micro/nanostructures on GaAs, Si, and brass," Opt. Express **18**(S4), A600–A619 (2010).

14. D. R. Austin, K. R. Kafka, Y. H. Lai, Z. Wang, C. I. Blaga, and E. A. Chowdhury, "Femtosecond laser damage of germanium from near-to mid-infrared wavelengths," Opt. Lett. **43**(15), 3702–3705 (2018).

15. A. Borowiec and H. Haugen, "Subwavelength ripple formation on the surfaces of compound semiconductors irradiated with femtosecond laser pulses," Appl. Phys. Lett. **82**(25), 4462–4464 (2003).

16. Y. Chai, X. Yu, H. Cheng, A. Chew, Z. Chang, M. Bass, and M. Soileau, "Single-shot intense few-cycle pulse interaction with polycrystalline ZnSe," Opt. Lett. **45**(12), 3216–3219 (2020).

17. S. Mirov, V. Fedorov, I. Moskalev, M. Mirov, and D. Martyshkin, "Frontiers of mid-infrared lasers based on transition metal doped II–VI semiconductors," J. Lumin. **133**, 268–275 (2013).

18. X. Ren, L.H. Mach, Y. Yin, Y. Wang, and Z. Chang, "Generation of 1 kHz, 2.3 mJ, 88 fs, 2.5 µm pulses from a Cr 2+: ZnSe chirped pulse amplifier," Opt. Lett. **43**(14), 3381–3384 (2018).

19. Y. Yin, J. Li, X. Ren, K. Zhao, Y. Wu, E. Cunningham, and Z. Chang, "High-efficiency optical parametric chirped-pulse amplifier in BiB3O6 for generation of 3 mJ, two-cycle, carrier-envelope-phase-stable pulses at 1.7 µm," Opt. Lett. **41**(6), 1142–1145 (2016).

20. H. Oczkowski and Z. Popławski, "Orientation of ZnSe crystals by chemical etching technique," J. Cryst. Growth **23**(2), 154–156 (1974).

21. X. Chen and R. Gaume, "Non-stoichiometric grain-growth in ZnSe ceramics for χ (2) interaction," Opt. Mater. Express **9**(2), 400–409 (2019).

22. G. Russell, M. Robertson, B. Vincent, and J. Woods, "An electron beam induced current study of grain boundaries in zinc selenide," J. Mater. Sci. **15**(4), 939–944 (1980).

23. P. A. Temple and M. J. Soileau, "Polarization Charge Model for Laser-Induced Ripple Patterns in Dielectric Materials," IEEE J. Quantum Electron. **17**(10), 2067–2072 (1981).

24. M. Huang, F. Zhao, Y. Cheng, N. Xu, and Z. Xu, "Origin of laser-induced near-subwavelength ripples: interference between surface plasmons and incident laser," ACS Nano **3**(12), 4062–4070 (2009).

25. S. Z. Xu, T. Q. Jia, H. Y. Sun, C. B. Li, X. Li, D. H. Feng, J. R. Qiu, and Z. Z. Xu, "Mechanisms of femtosecond laser-induced breakdown and damage in MgO," Opt. Commun. **259**(1), 274–280 (2006).

26. T. Jia, H. Chen, M. Huang, F. Zhao, J. Qiu, R. Li, Z. Xu, X. He, J. Zhang, and H. Kuroda, "Formation of nanogratings on the surface of a ZnSe crystal irradiated by femtosecond laser pulses," Phys. Rev. B **72**(12), 125429 (2005).

27. J. Bonse, J. Wrobel, K.-W. Brzezinka, N. Esser, and W. Kautek, "Femtosecond laser irradiation of indium phosphide in air: Raman spectroscopic and atomic force microscopic investigations," Appl. Surf. Sci. **202**(3-4), 272–282 (2002).

28. S. J. Yu, H. Asahi, S. Emura, H. Sumida, S. I. Gonda, and H. Tanoue, "Study of Ga ion implantation damage and annealing effect in Sn-doped InP using Raman scattering," J. Appl. Phys. **66**(2), 856–860 (1989).

29. K. Takimoto, A. Fukuta, Y. Yamamoto, N. Yoshida, T. Itoh, and S. Nonomura, "Linear thermal expansion coefficients of amorphous and microcrystalline silicon films," J. Non-Cryst. Solids **299-302**, 314–317 (2002).

30. C. Greiner, J. R. Felts, Z. T. Dai, W. P. King, and R. W. Carpick, "Local Nanoscale Heating Modulates Single-Asperity Friction," Nano Lett. **10**(11), 4640–4645 (2010).